Journal of Applied Pharmaceutical Science Vol. 12(08), pp 036-047, August, 2022
Available online at http://www.japsonline.com
DOI: 10.7324/JAPS.2022.120805
ISSN 2231-3354

Establishing a parallel compound screening method and identifying novel antimicrobial compounds targeting *Staphylococcus aureus* dihydrofolate reductase

Junpei Nakashima, Masamune Takeuchi, Shuhei Kawamoto, Kohei Monobe, Junichi Taira, Shunsuke Aoki*
Department of Bioscience and Bioinfomatics, Graduate School of Computer Science and System Engineering, Kyushu Institute of Technology, Iizuka, Japan.

ARTICLE INFO

Received on: 12/02/2022
Accepted on: 13/05/2022
Available Online: 04/08/2022

Key words:
DHFR, *Staphylococcus aureus*, antibiotics, structure-based drug screening, parallel compound screening, molecular dynamics.

ABSTRACT

The emergence of drug-resistant *Staphylococcus aureus* strains, such as methicillin-resistant *S. aureus* and vancomycin-resistant *S. aureus*, and their spread not only inside hospitals but also outside hospitals has become a major problem worldwide. In this study, we investigated novel antimicrobial compounds targeting trimethoprim-resistant *S. aureus* dihydrofolate reductase (TMP-resistant saDHFR). A novel screening method, called the parallel compound screening (PCS) method, was established to analyze a common population of compounds that showed top scores using two docking tools, GOLD and AutoDock Vina. Using 154,118 compounds in the structural library, we conducted a three-step *in silico* structure-based drug screening, including PCS, and identified nine candidate compounds targeting TMP-resistant saDHFR. The growth inhibitory effects of the candidate compounds on bacteria were examined on *Staphylococcus epidermidis*, a model microbial strain of *S. aureus*. Among the candidate compounds, two compounds showed strong growth inhibition against *S. epidermidis*. The IC_{50} values of the two compounds (6.34 and 56.94 μM) were determined. Molecular dynamics simulations predicted the direct and stable interactions between the active compounds and TMP-resistant saDHFR. The data regarding these active compounds from this study are expected to contribute to the development of new antibacterial agents against drug-resistant strains of *S. aureus*.

INTRODUCTION

Staphylococcus aureus (*S. aureus*) is a Gram-positive bacterium found on human skin and nasal cavity and causes pyogenic disease, sepsis, osteomyelitis, and endocarditis (Lakhundi and Zhang, 2018). Methicillin-resistant *S. aureus* (MRSA) and vancomycin-resistant *S. aureus* (VRSA) cause nosocomial infections (McGuinness *et al*., 2017). These resistant strains are not confined only to hospitals but have also spread in the community (community-acquired MRSA: caMRSA) (Khan *et al*., 2018). The caMRSA infection causes serious diseases such as necrotizing pneumonia and can be life-threatening. An outbreak of this species affected several people in the early 2000s, and the disease spread worldwide. The spread of caMRSA infections is predicted to become a major problem in the future (Khan *et al*., 2018).

The *de novo* synthesis pathway, a nucleic acid synthesis pathway in *S. aureus*, produces the purine nucleotides ATP and GTP (Li *et al*., 2011). Inhibition of this pathway leads to decreased nucleic acid synthesis, which ultimately kills bacteria (Kobayashi *et al*., 2014). Dihydrofolate reductase (DHFR), which is involved in the *de novo* synthesis pathway, is a known target for developing antibacterial drugs and is gathering attention as an attractive drug target against MRSA and VRSA (He *et al*., 2020; Kobayashi *et al*., 2014). Trimethoprim (TMP) is a classical DHFR-targeting antimicrobial agent used to treat infections caused by *S. aureus*. TMP is prescribed together with sulfamethoxazole (SMX) as co-trimoxazole (Bactrim) to prevent the emergence of resistant mutations in bacteria (Wróbel *et al*., 2020). SMX is a specific

*Corresponding Author
Shunsuke Aoki, Department of Bioscience and Bioinformatics, Graduate School of Computer Science and Systems Engineering, Kyushu Institute of Technology, Iizuka 820 8502, Japan.
E-mail: aokis @ bio.kyutech.ac.jp

inhibitor of the dihydropteroate synthesis (DHPS) enzyme. It has been reported that the Phe98 group in DHFR is mutated to Tyr (F98Y) in many pathogenic *S. aureus* variants (Wang *et al*., 2022). *Staphylococcus aureus* with mutated DHFR developed resistance to the diaminopyrimidine (DAP) ring of TMP. Therefore, identifying compounds different from TMP and those that are devoid of the DAP ring would help develop new therapeutic agents for patients infected with TMP-resistant *S. aureus* strains, as well as MRSA, VRSA, and caMRSA strains (Holland *et al*., 2014). Drug discovery targeting TMP-resistant *S. aureus* DHFR (TMP-resistant saDHFR) has attracted a great deal of attention (Huang *et al*., 2019; Keshipeddy *et al*., 2015; Reeve *et al*., 2019; Wang *et al*., 2022).

Structure-based drug screening (SBDS) has remained one of the most effective computational methods for developing new drugs (Pinzi and Rastelli, 2019). Based on the three-dimensional structure of the target protein, chemical compounds that bind to the pocket structure of the target were searched using protein-compound docking tools. *In silico* SBDS was performed using docking simulation tools such as GOLD (Scarpino *et al*., 2018), DOCK (Kinjo *et al*., 2013), GLIDE (Reddy *et al*., 2020), FRED (Gentile *et al*., 2020), AutoDock Vina (Trott and Olson, 2010), and Hex (Uciechowska-Kaczmarzyk *et al*., 2019). Multistep *in silico* SBDS, which consists of two or more docking simulation tools, has been used as a more effective way to identify active compounds (Taira *et al*., 2017). In particular, a high hit rate can be achieved by utilizing a compound screening method in which multiple docking simulations are linked hierarchically (Kobayashi *et al*., 2014; Kuriki *et al*., 2021).

The emergence of drug-resistant strains threatens the pool of first-line drugs, and this issue has necessitated the rapid and continuous development of novel antimicrobial agents. Computer-aided drug discovery provides a solution because, in comparison with screening based on biological experiments, the technique enables a more rapid identification of lead compounds. However, there is still room to improve efficiency in distinguishing true or false positives. In this study, the structure of TMP-resistant saDHFR was used as a target protein to identify novel antimicrobial compounds that are effective against multidrug-resistant *S. aureus* strains. Many attempts at hierarchical *in silico* drug screening have been made (Pinzi and Rastelli, 2019). This study reports the parallel use of two flexible docking simulation tools based on genetic algorithms. We established an AutoDock Vina (ADV)-GOLD parallel compound screening (PCS) method and identified novel antimicrobial chemical compounds. The dose-dependent inhibitory effects of the active compounds were confirmed and IC_{50} values were determined. The molecular dynamics (MD) simulation results indicated that the compounds directly interacted with TMP-resistant saDHFR.

MATERIALS AND METHODS

Compound structure library

The three-dimensional structural compound library (154,118 compounds from ChemBridge) was obtained from the Ressource Parisienne en Bioinformatique Structurale (RPBS) web-based database [available at http://bioserv.rpbs.jussieu.fr/RPBS/cgi-bin/Ressource.cgi?chzn_lg=an&chzn_rsrc=Collections (accessed Jun 10, 2012)]. The compound library was filtered using ADME/Tox filters to exclude compounds that were inappropriate as drugs. Compound structure libraries with multiple conformations were created, with a maximum of 10 conformations per compound. Compound multicoordinates were generated using the LowModeMD method (Labute, 2010).

Crystal structures of target proteins

The X-ray crystal structure of DHFR (PDB ID: 3M09) of the TMP-resistant *S. aureus* used in this study was obtained from the Research Collaboratory for Structural Bioinformatics Protein Data Bank (PDB) [available at https://www.rcsb.org/ (accessed May 15, 2017)].

Molecular surface extraction and pocket search

The protein structure of 3M09 was downloaded and calculations were performed to add hydrogen atoms and charges to the 3D structure of DHFR, as described in a previous study (Kuriki *et al*., 2021). Before performing the *in silico* SBDS, molecular surface extraction and pocket searches were performed. We used the DMS program to extract the molecular surface and the sphgen program to search for pockets [(available at https://dock.compbio.ucsf.edu/ (accessed April 2, 2017)]. The protein–ligand interaction (LI) region was restricted to the region close to the active site of the TMP-resistant saDHFR. $NADP^+$, a coenzyme of DHFR, was prebound to the protein and other ligands were excluded.

Three-step hierarchical *in silico* SBDS with PCS method

In silico SBDS was performed using DOCK version 6.4, GOLD suite version 5.2.2, and ADV 1.1.2. DOCK, a grid docking tool that was used for the first screening. The scoring function of DOCK was calculated by predicting the protein–ligand binding affinity using van der Waals and electrostatic interaction energies. The binding affinities between the protein and the compounds selected in the first screening were evaluated using the genetic algorithm (GA) flexible docking simulation tools GOLD and ADV in the second screening effort. In the third screening, although the screening system was the same as in the second screening, docking simulation was performed for a 3D compound library with multiple configurations (compounds selected from the second screening). Finally, the compounds were filtered based on the following criteria: the score of the postscoring function RF-ScoreVS (Wang and Zhang, 2017), the presence of important interactions, and Lipinski's rule of five (Lipinski *et al*., 2012).

Compounds

All candidate compounds (JP1–9) used in this study were purchased from ChemBridge Corporation (San Diego, CA) and dissolved in dimethyl sulfoxide (DMSO, Sigma). Table 1 lists the compound numbers, names, and ChemBridge IDs.

Bacterial species and growth inhibition assay

Staphylococcus epidermidis was purchased from the Microbial Materials Development Laboratory, RIKEN BioResource Center (Saitama, Japan). *S. epidermidis* was cultured overnight in 2 ml of the culture medium [composition: 1% peptone (BD), 1% beef extract (BD), and 0.5% NaCl (Wako, Japan), adjusted to pH 6.9] at 37°C and 240 rpm. The cultured *S. epidermidis* cells were diluted 52-fold and seeded in 96-well

Table 1. Details of the compounds used in this study.

Name	IUPAC name	ID
JP1	2-Methyl-5-(4-{[4-(1-piperidinylcarbonyl)phenyl]amino}-1-phthalazinyl)benzenesulfonamide	6339168
JP2	N-(2,3-Dimethylphenyl)-2-{[1-(1-naphthyl)-1H-tetrazol-5-yl]thio}acetamide	6566533
JP3	N-(5-Benzoyl-2-hydroxybenzyl)-2-[(5-benzyl-4-methyl-4H-1,2,4-triazol-3-yl)thio]acetamide	7013416
JP4	2-Imino-10-methyl-5-oxo-N-(1-phenylethyl)-1-(3-pyridinylmethyl)-1,5-dihydro-2H-dipyrido[1,2-a:2',3'-d] pyrimidine-3-carboxamide	7172775
JP5	N-(4-{[(5-Methyl-3-isoxazolyl)amino]sulfonyl}phenyl)-2-phenyl-2-(phenylthio)acetamide	7294426
JP6	4-({2-[(3-Methylbenzoyl)amino]benzoyl}amino)benzoic acid	7319967
JP7	2-[(4,6-Dianilino-1,3,5-triazin-2-yl)thio]-N-(2-methoxyphenyl)acetamide	7704952
JP8	3-[5-({2-[(Diphenylmethyl)amino]-2-oxoethyl}thio)-1H-tetrazol-1-yl]benzoic acid	7919462
JP9	3-[5-(3-{[(2-Methoxyphenoxy)acetyl]amino}phenoxy)-1,3-dioxo-1,3-dihydro-2H-isoindol-2-yl]propanoic acid	7968035

plates under 3 conditions: 0.3% DMSO (negative control), ampicillin (positive control), and the candidate compound. After 6 h of incubation at 37°C and 240 rpm, the turbidity (OD_{595}) of the culture medium was measured using a microplate reader (Bio-Rad Laboratories, Inc., Hercules, CA).

Molecular dynamics simulation

MD simulations were performed using the ligand–protein complex structures predicted by GOLD docking simulations. The GROMACS package with the CHARMM36m force field was used as the MD tool [available at: https://www.gromacs.org// (accessed Jan 15, 2020)]. A simulation system consisting of proteins, compounds, water molecules, and ions was constructed using the CHARMM-GUI web server [available at https://www.charmm-gui.org/ (accessed Feb 15, 2021)]. TIP3P was used as a water molecule. The cut-off distance for the van der Waals force and electrostatic interaction between the atoms was 1.2 nm. The particle mesh Ewald method was used to calculate long-range electrostatic interactions. The LINCS constraint algorithm was used for the energy minimization, equilibration, and production MD calculations. Energy minimization calculations were carried out in up to 5,000 steps using the steepest descent algorithm. Equilibration calculations were then carried out in one step under NVT conditions (310.15 K), followed by two steps under NPT conditions (310.15 K, 1 bar). Finally, 30 ns production MD calculations were performed with a time step of 2 fs. MD trajectories were analyzed using g_rms in the GROMACS package.

Statistical analysis

All statistical analyses were performed using R (The R Foundation for Statistical Computing, Vienna, Austria) and GraphPad Prism (GraphPad Prism Software, Inc., San Diego, CA).

RESULTS

The parallel compound screening method

We established the PCS method using the GA docking tools GOLD and ADV. This method selects a common population of compounds ranked in the top scores of the two docking tools. The datasets in the useful (docking) decoys-enhanced (DUD-E) database [available at http://dude.docking.org/ (accessed Jun 24, 2019)] were used for accuracy validation (Mysinger *et al*., 2012). The DUD-E database contained 102 target protein structures and datasets of their active and inactive ligand structures. To evaluate the prediction performance of docking simulation tools, the docking score values were analyzed using the receiver operating characteristic (ROC) curve and the area under the curve values. PCS is a method of binarization (classification) based on whether the compound is in the common population, and it does not provide specific parameters. Thus, the ROC curve analysis cannot be used to validate the accuracy of the PCS method. Therefore, the PCS method was evaluated using enrichment factor (EF) and success rate (SR) values (Wang and Zhang, 2017). The EF is a measure of the number of active compounds included in candidate compounds. The SR is a measure that calculates the proportion of proteins in a group of target proteins for which at least one active ligand is obtained. The accuracy of the PCS method was verified for all 102 target proteins in the DUD-E. We used a 200-compound dataset consisting of 20 true-active ligands and 180 pseudo-active compounds (decoys) that are similar to the active ligands but did not bind to the protein for each target protein. The results are presented in Table S1. The percentage of the EF2% (PCS) ≥ EF2% (GOLD) group was 74.5%, and the percentage of EF2% (PCS) ≥ EF2% (ADV) was 82.4%. The SR values for the GOLD, ADV, and PCS methods were 81.4, 83.3, and 85.3%, respectively. In terms of both EF2% and SR, the PCS method performed better than GOLD and ADV. Among the two indicators, the PCS method showed superior performance compared to the conventional method GOLD alone and ADV alone.

Three-step hierarchical *in silico* SBDS including PCS

A 3-step hierarchical *in silico* SBDS approach (Fig. 1) was used to screen 154,118 compounds in the structural library [available at http://bioserv.rpbs.jussieu.fr/RPBS/cgi-bin/Ressource.cgi?chzn_lg=an&chzn_rsrc=Collections (accessed Jun 10, 2012)] for TMP-resistant saDHFR (PDB ID: 3M09). In the first screening, rigid grid-docking simulations were performed using DOCK. In the second screening, we used the GA-based docking tools, GOLD and ADV in parallel, to screen compounds in singular coordination using the PCS method. In the third screening, the same PCS method as that in the second screening was applied to compounds with multiple conformers. The interactions between the protein and compound were then checked using the LI tool

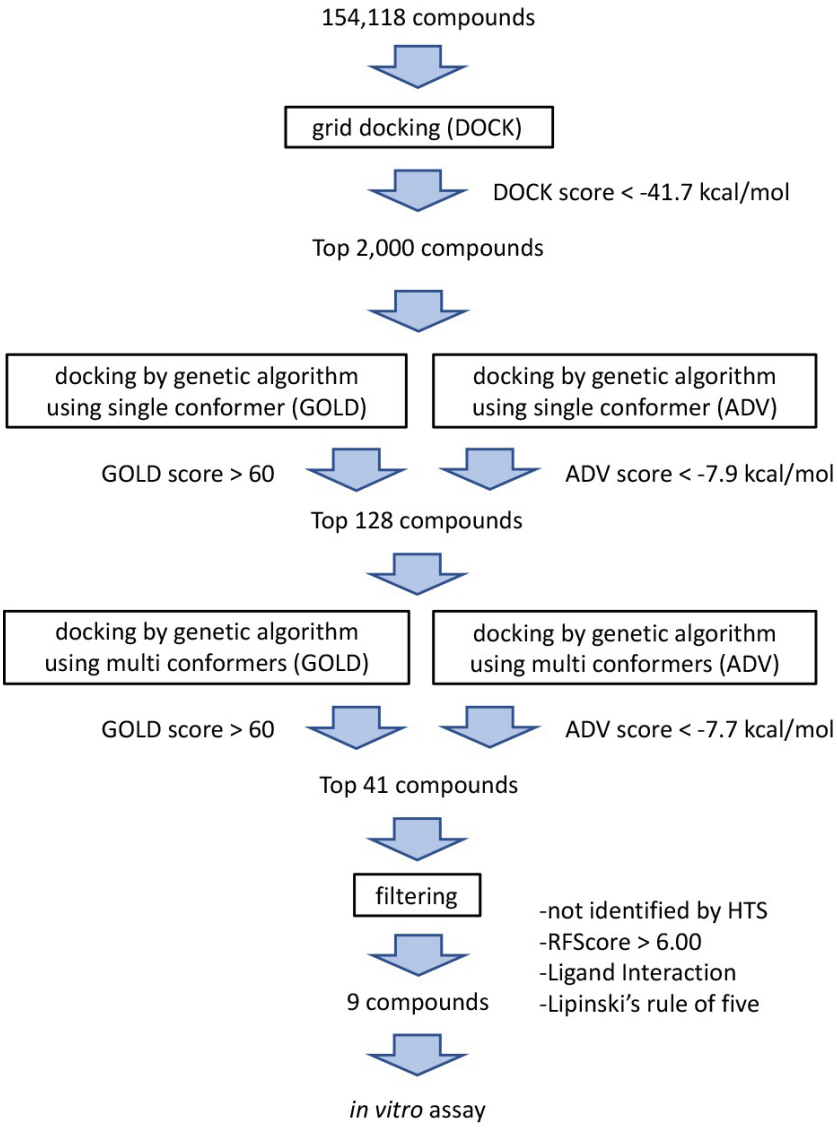

Figure 1. Flowchart of the three-step hierarchical *in silico* SBDS with PCS method.

as a filter to confirm the binding mode near the pocket (Ahmed *et al*., 2021). The RF score was then calculated using RF-Score-VS (Wang and Zhang, 2017) using GOLD scores, a postscoring function that uses machine learning. Finally, the compounds were filtered by applying Lipinski's rule of five. The final selected nine compounds are listed in Table 1. Table 2 presents the GOLD and ADV scores for each compound.

Bacterial growth inhibition assay for the candidate compounds

Nine candidate compounds (named JP1–9) predicted via the three-step hierarchical *in silico* SBDS were analyzed for their growth inhibitory effects on bacteria. *S. epidermidis* (biosafety level 1) was used as a model *S. aureus* bacterium in this growth inhibition assay (Kobayashi *et al*., 2014) because our laboratory is not equipped to perform experiments using *S. aureus* (biosafety level 2). The amino acid sequences of TMP-resistant *sa*DHFR and

Table 2. Score values for the nine candidate compounds identified by SBDS with the PCS method.

Name	GOLD score[a]	ADV score[a]
JP1	75.65 ± 1.83	−10.11 ± 0.48
JP2	64.42 ± 1.49	−9.01 ± 0.3
JP3	80.56 ± 3.4	−9.27 ± 0.05
JP4	67.72 ± 0.96	−9.45 ± 0.14
JP5	84.81 ± 1.61	−9.26 ± 0.07
JP6	71.82 ± 1.37	−9.27 ± 0.23
JP7	78.88 ± 3.53	−8.95 ± 0.07
JP8	75.12 ± 1.17	−9.4 ± 0.13
JP9	80.58 ± 5.6	−9.29 ± 0.35

[a]Each value represents mean ± standard error.

S. epidermidis DHFR were analyzed using BLAST [available at https://blast.ncbi.nlm.nih.gov/Blast.cgi (accessed Aug 20, 2017)] and UniProt [available at https://www.uniprot.org/ (accessed Aug 20, 2017)]. The residues near the active site of TMP-resistant saDHFR were completely conserved in *S. epidermidis*, and the RMSD value between both protein structures was 0.543 Å (Kobayashi *et al*., 2014). JP5 and JP9 showed a strong inhibitory effect among the candidate compounds, while JP7 showed a weak inhibitory effect (Fig. 2). Figure 3A–C shows the structures of the three compounds that had an inhibitory effect on bacterial growth, and these three compounds were not structurally similar to each other. Both GOLD and ADV predicted that all three compounds would bind close to the active site of the DHFR (Fig. 3D–F, data of ADV not shown). The dose-dependent effects of two compounds (JP5 and JP9) on the growth of *S. epidermidis* were investigated. The IC_{50} value of JP9 was 6.34 ± 0.47 µM, while the effect was weaker for JP5, with an IC_{50} value of 56.94 ± 3.16 µM (Fig. 4).

Binding mode prediction of the hit compounds

The interactions between TMP-resistant saDHFR and hit compounds (JP5 and JP9) were evaluated using the LI and protein–LI fingerprint (PLIF; data not shown) tools in Molecular Operating Environment (MOE) version 2011. 10 (Ahmed *et al*., 2021). Figure 5 shows the binding mode predictions by LI using the ligand–protein complex structures with the highest score calculated by GOLD in the third screening step. All hit compounds were located near the active site of DHFR (Fig. 3D–F). The results of the combined LI and PLIF analyses using multiple conformers are shown in Table 3. The analyses suggested that both the active compounds interacted with Phe92 (Fig. 5 and Table 3). JP5 appeared to form a hydrogen bond with Phe92, and JP9 binds to Phe92 via arene–arene interaction. The benzyl group of JP5 formed a hydrogen bond with Leu28, and the carboxyl and amide groups of JP9 formed a hydrogen bond with His30 and Leu20, respectively. In addition, PLIF analysis with

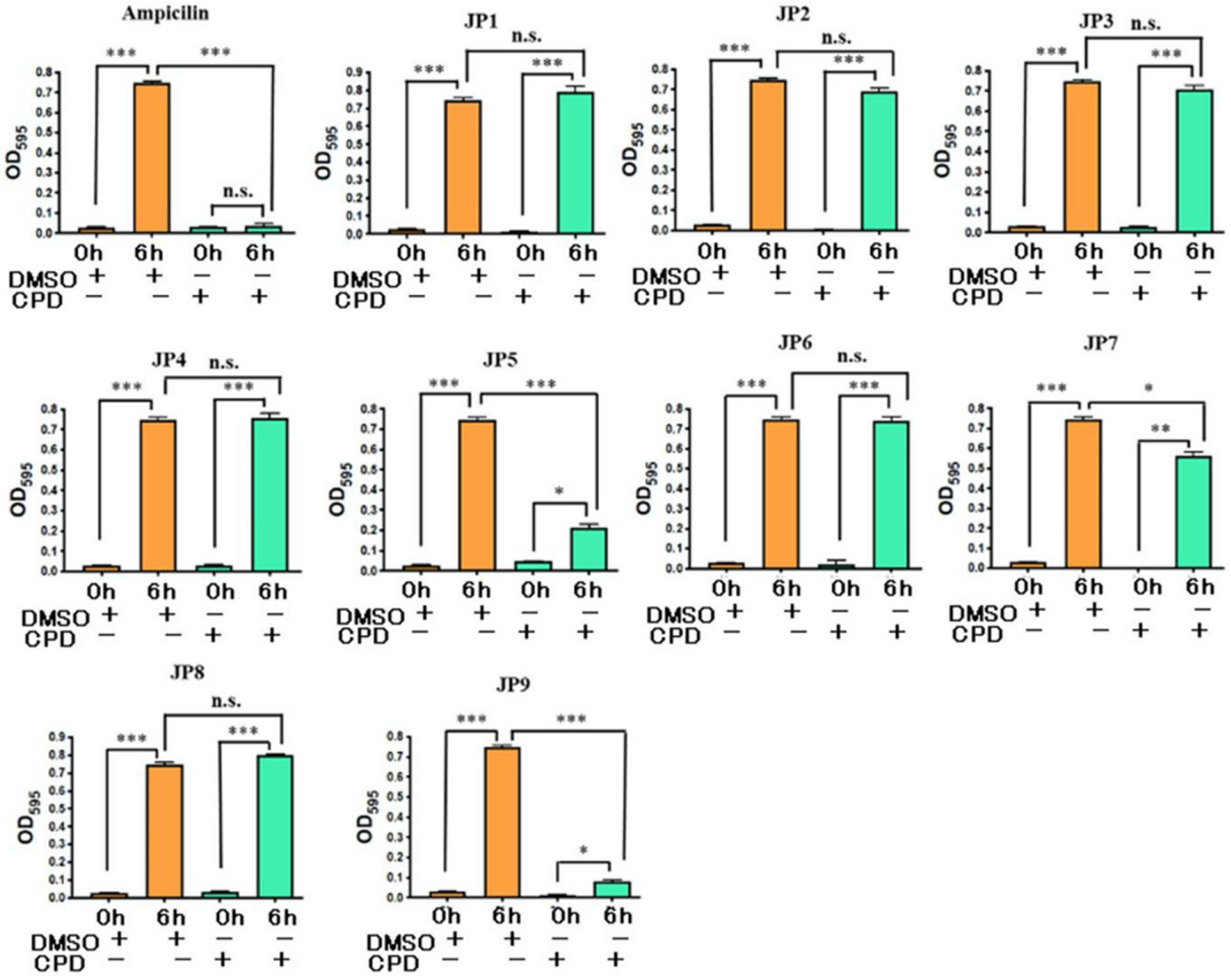

Figure 2. Results of growth inhibition assay of *S. epidermidis* by candidate compounds (JP1–9). The concentration of all compounds was 100 µM. DMSO (0.3%) and ampicillin (100 µg/mL) were used as the negative and positive controls, respectively. All values represent mean ± SEM of four independent experiments. Bonferroni's all-pairs comparison test was performed (n.s.: not significant; ***: $p < 0.001$; **: $p < 0.002$; *: $p < 0.033$). CPD: compound.

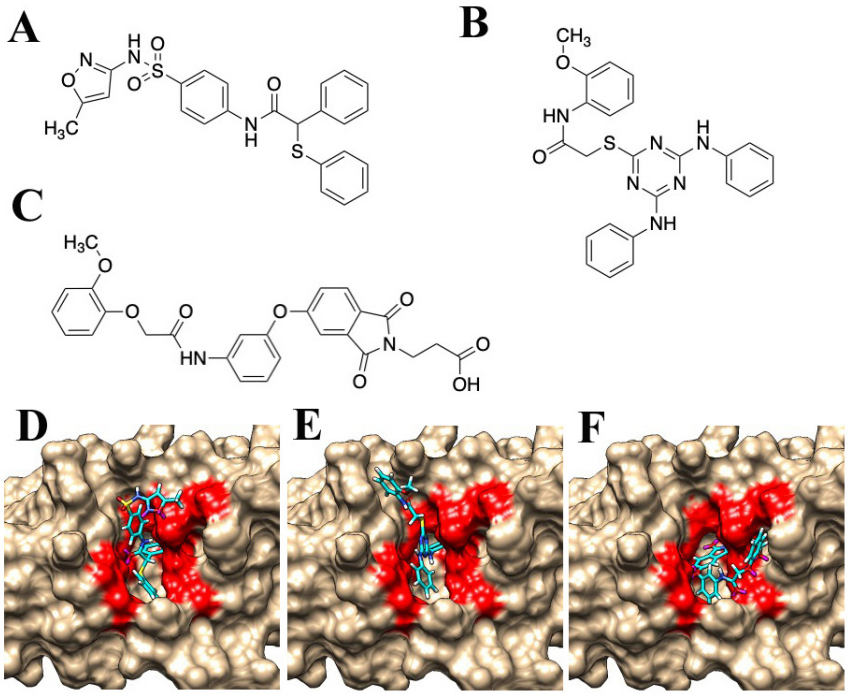

Figure 3. Structures of the compounds with antibacterial activity. (A) JP5, (B) JP7, and (C) JP9. The complex structures of compounds and the TMP-resistant saDHFR are shown in (D–F). (D) JP5–TMP-resistant saDHFR. (E) JP7–TMP-resistant saDHFR. (F) JP9–TMP-resistant saDHFR. The amino acid residues of the active site pockets are shown in red color.

multiple conformers revealed the potential interactions of JP9 with Val6, His23, Asp27, and Thr11 (Table 3).

Analysis of compound-protein interaction by MD simulation

MD simulations of 30 ns were performed using the ligand–protein complex structures, JP5–TMP-resistant saDHFR, and JP9–TMP-resistant saDHFR, predicted by GOLD in the third screening. The 30 ns simulations with the complex structure of the TMP–TMP-resistant saDHFR protein were also performed. The complex structure was generated by docking simulation using GOLD (GOLD score = 67.70). A previous study showed that ligand binding ability could be assessed with high accuracy by analyzing ligand RMSD values in MD simulations with 56 proteins and 569 ligands (Guterres and Im, 2020). The time-dependent change of ligand RMSD value was analyzed for 30 ns production MD simulations, and the ligand RMSD value of TMP exceeded 0.65 nm by 2 ns and then exceeded 1.0 nm after 16 ns. At 2 ns, TMP dissociated from the active site pocket and never returned to the pocket. The mean RMSD value of TMP was 0.66 nm, indicating that TMP does not bind to the TMP-resistant saDHFR protein stably. On the contrary, the ligand RMSD values of JP5 and JP9 were stable throughout the simulation, with mean ligand RMSD values of 0.25 nm and 0.27 nm, respectively, indicating that JP5 and JP9 may stably and directly bind to the TMP-resistant saDHFR protein.

Toxicity assessment using the toxicity prediction tools

The toxicities of the candidate compounds were assessed by calculating the predicted LD_{50} values for oral administration in rats using TEST, a toxicity prediction tool [available at http://www.epa.gov/nrmrl/std/qsar/qsar.html (accessed Aug 20, 2020)]. TEST predicted LD_{50} values of 1902.8 and 3147.1 mg/kg body weight for JP5 and JP9, respectively. JP5 and JP9 were predicted to have sufficiently low toxicity compared with TMP (LD_{50} = 1648.1 mg/kg body weight). ToxiM, a machine learning-based toxicity prediction tool, estimated the toxicity classification scores of JP5, JP9, and TMP (Sharma *et al*., 2017). The toxicity scores of JP5, JP9, and TMP were 0.978, 0.860, and 0.926, respectively, suggesting that JP9 was less toxic than TMP.

DISCUSSION

We constructed and validated a novel screening method, the PCS method, and found that it performed better than the conventional methods. PCS was incorporated into the screening pathway targeting TMP-resistant saDHFR, and three compounds with growth inhibitory effects on *S. epidermidis* were identified. The interactions of the compounds (JP5 and JP9) identified in this study were predicted by LI and PLIF analyses. JP5 was predicted to form a hydrogen bond with Leu28, which is the same as that of TMP (Kobayashi *et al*., 2014). The significance of the Leu20 interaction in wild-type saDHFR has also been reported in previous studies investigating other inhibitory compounds (Kobayashi *et al*., 2014). LI analysis also predicted an interaction between JP9 and His30. These are likely to explain the difference in the growth inhibitory effects of JP5 and JP9. Leu20 is considered an important residue not only in wild-type saDHFR but also in TMP-resistant saDHFR. Furthermore, compounds with growth inhibitory effects commonly interact with Phe92. Therefore, interactions with

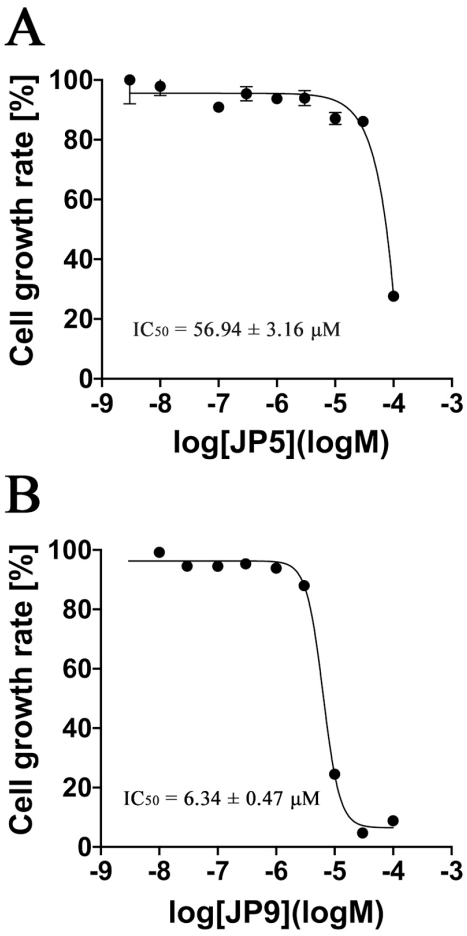

Figure 4. Results of the verification of the dose-dependent effect of JP5 and JP9 on the growth of *S. epidermidis*. The vertical axis represents the bacterial growth rate (%) of *S. epidermidis* after 6 hours of incubation, and the horizontal axis represents the concentration of each compound on a logarithmic scale (log M). Each plot represents mean ± SEM of four independent experiments. The IC_{50} values were determined using nonlinear regression analysis. Each IC_{50} value was determined using four independent experiments and nonlinear regression analysis. (A) JP5 and (B) JP9.

Leu20, His30, and Phe92 are likely to be important for inhibiting the enzyme activity of DHFR.

There exists compatibility between docking simulation tools and target proteins (Pereira *et al*., 2016). Hence, selecting an appropriate tool for each target protein is important to identify hit compounds with a high probability. However, in the absence of a sufficient dataset, the ROC curve analysis cannot be used to assess the validity of a target protein/tool combination. Even in the absence of a sufficient ligand dataset, the PCS method can provide information on the compatibility between the docking tool and target protein. If the percentage of common compounds in the total compounds selected by each of the two tools is zero or very low, then it indicates that one or both tools may not be suitable for evaluating the target protein. Such information on the compatibility between target proteins and tools is extremely important for planning strategies for *in silico* drug discovery.

MD simulations using the complex structures of JP5 and JP9 with TMP-resistant saDHFR showed that the complexes remained stable for 30 ns with low RMSD values, suggesting that JP5 and JP9 can bind directly to TMP-resistant saDHFR. On the contrary, TMP deviated from the active site pocket of the TMP-resistant saDHFR early during the 30 ns MD simulation and did not return to the pocket. JP9 inhibited the growth of the bacteria at low concentrations (IC_{50} value = 6.34 μM) and was also predicted to be less toxic than TMP by the two independent tools for toxicity prediction. Considered together, multiple lines of evidence from *in silico* simulations and *in vitro* experiments suggest that JP9 is a promising molecule for future antimicrobial drug development. The hit rate of the three-step *in silico* SBDS method with the newly proposed screening system with PCS was 22% (33%, including the one that showed weak growth inhibition). This hit rate is extremely high compared to experimental high-throughput screening. Not only the active compounds but also the compound that showed only a weak growth inhibition effect is likely useful as lead compounds for the next step of drug discovery, which is to search for analogues with modified functional groups. The three-step *in silico* SBDS method used in this study is thought to be effective in terms of both time and cost for identifying new active lead compounds.

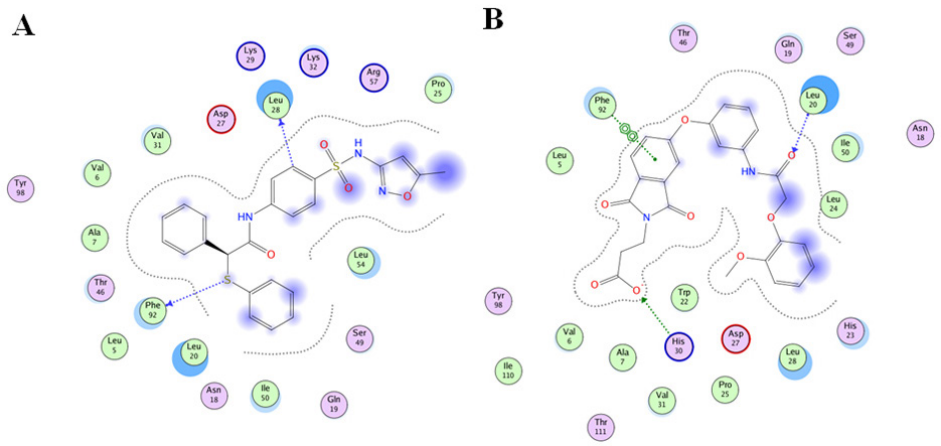

Figure 5. Binding mode prediction of TMP-resistant saDHFR and hit compounds using LI.
(A) JP5 and (B) JP9. Purple circles: polar amino acids. Green circles: hydrophobic amino acids. Green and blue dotted arrows are side chain and backbone hydrogen bonds, respectively. Green double benzene indicates arene–arene interaction. Blue blurred regions indicate ligand exposure atoms.

Table 3. Predicted interaction residues of the compounds by PLIF or LI analyses.

Name	Predicted interacting residues (LI or PLIF)
JP5	Leu28, Phe92
JP9	Leu20, His30, Phe92 or Val6, His23, Asp27, Thr111

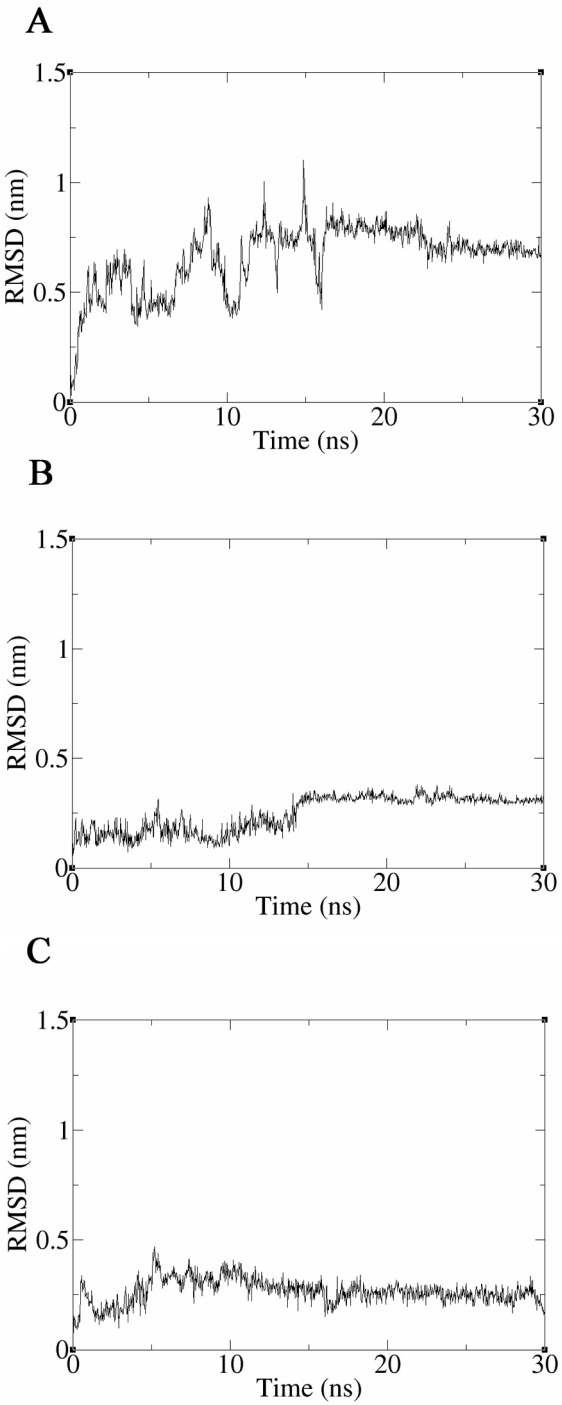

Figure 6. Results of the interaction analysis between TMP-resistant saDHFR and compounds using MD simulations. Time-dependent changes of ligand RMSD values for TMP (A), JP5 (B), and JP9 (C) during 30 ns production MD simulations. The vertical and horizontal axes represent the ligand RMSD (nm) and time (ns), respectively.

CONCLUSION

In this study, compared with the conventional strategy, the PCS method exhibited advantages in the two metrics, EF2% and SR, and out of nine experimentally validated candidates, JP5 and JP9 were identified as active inhibitors. Furthermore, the MD simulation strongly suggested that JP5 and JP9 can form stable complexes with the active sites in TMP-resistant saDHFR. Considering that JP5 and JP9 have unique structures, these compounds could be novel leads for anti-infectives against *S. aureus* with TMP resistance. In the context of effectively identifying lead compounds, we believe that integrating the PCS method into an *in silico* SBDS platform could improve the computer-assisted strategy of identifying competitive inhibitors.

ACKNOWLEDGMENTS

This work was supported in part by a Grant-in-Aid for Scientific Research (26460145) from the Ministry of Education, Culture, Sports, Science, and Technology of Japan. The authors thank Kohei Kuriki for his descriptive support.

AUTHOR CONTRIBUTIONS

All authors made substantial contributions to conception and design, acquisition of data, or analysis and interpretation of data; took part in drafting the article or revising it critically for important intellectual content; agreed to submit to the current journal; gave final approval of the version to be published; and agree to be accountable for all aspects of the work. All the authors are eligible to be an author as per the international committee of medical journal editors (ICMJE) requirements/guidelines.

CONFLICTS OF INTEREST

The authors report no financial or any other conflicts of interest in this work.

ETHICAL APPROVALS

This study does not involve experiments on animals or human subjects.

DATA AVAILABILITY

All data generated and analyzed are included within this research article.

PUBLISHER'S NOTE

This journal remains neutral with regard to jurisdictional claims in published institutional affiliation.

REFERENCES

Ahmed MF, Santali EY, El-Haggar R. Novel piperazine-chalcone hybrids and related pyrazoline analogues targeting VEGFR-2 kinase; design, synthesis, molecular docking studies, and anticancer evaluation. J Enzyme Inhib Med Chem, 2021; 36:307–18.

Gentile F, Agrawal V, Hsing M, Ton A-T, Ban F, Norinder U, Gleave ME, Cherkasov A. Deep docking: a deep learning platform for augmentation of structure based drug discovery. ACS Cent Sci, 2020; 6:939–49.

Guterres H, Im W. Improving protein-ligand docking results with high-throughput molecular dynamics simulations. J Chem Inf Model, 2020; 60:2189–98.

He J, Qiao W, An Q, Yang T, Luo Y. Dihydrofolate reductase inhibitors for use as antimicrobial agents. Eur J Med Chem, 2020; 195.

Holland TL, Arnold C, Fowler VG. Clinical management of *Staphylococcus aureus* bacteremia: a review. JAMA, 2014; 312:1330–41.

Huang DB, Noviello S, Balser B, Scaramucci A, Corey GR. A Pooled analysis of the safety and efficacy of iclaprim versus vancomycin for the treatment of acute bacterial skin and skin structure infections in patients with intravenous drug use: phase 3 REVIVE studies. Clin Ther, 2019; 41:1090–6.

Keshipeddy S, Reeve SM, Anderson AC, Wright DL. Nonracemic antifolates stereoselectively recruit alternate cofactors and overcome resistance in *S. aureus*. J Am Chem Soc, 2015; 137:8983–90.

Khan A, Wilson B, Gould IM. Current and future treatment options for community-associated MRSA infection. Expert Opin Pharmacother, 2018; 19:457–70.

Kinjo T, Koseki Y, Kobayashi M, Yamada A, Morita K, Yamaguchi K, Tsurusawa R, Gulten G, Komatsu H, Sakamoto H, Sacchettini JC, Kitamura M, Aoki S. Identification of compounds with potential antibacterial activity against Mycobacterium through structure-based drug screening. J Chem Inf Model, 2013; 53:1200–12.

Kobayashi M, Kinjo T, Koseki Y, Bourne CR, Barrow WW, Aoki S. Identification of novel potential antibiotics against *Staphylococcus* using structure-based drug screening targeting dihydrofolate reductase. J Chem Inf Model, 2014; 54:1242–53.

Kuriki K, Taira J, Kuroki M, Sakamoto H, Aoki S. Computer-assisted screening of mycobacterial growth inhibitors: Exclusion of frequent hitters with the assistance of the multiple target screening method. Int J Mycobacteriol, 2021; 10:307–11.

Labute P. LowModeMD–implicit low-mode velocity filtering applied to conformational search of macrocycles and protein loops. J Chem Inf Model, 2010; 50:792–800.

Lakhundi S, Zhang K. Methicillin-resistant *Staphylococcus aureus*: molecular characterization, evolution, and epidemiology. Clin Microbiol Rev, 2018; 31.

Li X, Hilgers M, Cunningham M, Chen Z, Trzoss M, Zhang J, Kohnen L, Lam T, Creighton C, G C K, Nelson K, Kwan B, Stidham M, Brown-Driver V, Shaw KJ, Finn J. Structure-based design of new DHFR-based antibacterial agents: 7-aryl-2,4-diaminoquinazolines. Bioorg Med Chem Lett, 2011; 21:5171–6.

Lipinski CA, Lombardo F, Dominy BW, Feeney PJ. Experimental and computational approaches to estimate solubility and permeability in drug discovery and development settings. Adv Drug Deliv Rev, 2012; 64:4–17.

McGuinness WA, Malachowa N, DeLeo FR. Vancomycin resistance in *Staphylococcus aureus*. Yale J Biol Med, 2017; 90:269–81.

Mysinger MM, Carchia M, Irwin JJ, Shoichet BK. Directory of useful decoys, enhanced (DUD-E): Better ligands and decoys for better benchmarking. J Med Chem, 2012;55:6582–94.

Pereira JC, Caffarena ER, dos Santos CN. Boosting docking-based virtual screening with deep learning. J Chem Inf Model, 2016; 56:2495–506.

Pinzi L, Rastelli G. Molecular docking: Shifting paradigms in drug discovery. Int J Mol Sci, 2019; 20.

Reddy KK, Rathore RS, Srujana P, Burri RR, Reddy CR, Sumakanth M, Reddanna P, Reddy MR. Performance evaluation of docking programs- glide, gold, autodock & surflexdock, using free energy perturbation reference data: a case study of fructose-1, 6-bisphosphatase-AMP analogs. Mini Rev Med Chem, 2020; 20:1179–87.

Reeve SM, Si D, Krucinska J, Yan Y, Viswanathan K, Wang S, Holt GT, Holt GT, Ojewole AA, Estrada A, Agabiti SS, Alverson JB, Gibson ND, Priestley ND, Wiemer AJ, Donald BR, Wright DL. Toward broad spectrum dihydrofolate reductase inhibitors targeting trimethoprim resistant enzymes identified in clinical isolates of methicillin resistant *Staphylococcus aureus*. ACS Infect Dis, 2019; 5:1896–906.

Scarpino A, Ferenczy GG, Keserű GM. Comparative evaluation of covalent docking tools. J Chem Inf Model, 2018; 58:1441–58.

Sharma AK, Srivastava GN, Roy A, Sharma VK. ToxiM: a toxicity prediction tool for small molecules developed using machine learning and chemoinformatics approaches. Front Pharmacol, 2017; 8.

Taira J, Morita K, Kawashima S, Umei T, Baba H, Maruoka T, Komatsu H, Sakamoto H, Sacchettini JC, Aoki S. Identification of a novel class of small compounds with anti-tuberculosis activity by *in silico* structure-based drug screening. J Antibiot (Tokyo), 2017; 70:1057–64.

Trott O, Olson AJ. AutoDock Vina: improving the speed and accuracy of docking with a new scoring function, efficient optimization, and multithreading. J Comput Chem, 2010; 31:455–61.

Uciechowska-Kaczmarzyk U, Chauvot de Beauchene I, Samsonov SA. Docking software performance in protein-glycosaminoglycan systems. J Mol Graph Model 2019; 90:42–50.

Wang C, Zhang Y. Improving scoring-docking-screening powers of protein-ligand scoring functions using random forest. J Comput Chem, 2017; 38:169–77.

Wang S, Reeve SM, Holt GT, Ojewole AA, Frenkel MS, Gainza P, Keshipeddy S, Fowler VG, Wright DL, Donald BR. Chiral evasion and stereospecific antifolate resistance in *Staphylococcus aureus*. PLoS Comput Biol, 2022; 18.

Wróbel A, Arciszewska K, Maliszewski D, Drozdowska D. Trimethoprim and other nonclassical antifolates an excellent template for searching modifications of dihydrofolate reductase enzyme inhibitors. J Antibiot (Tokyo), 2020; 73:5–27.

How to cite this article:
Nakashima J, Takeuchi M, Kawamoto S, Monobe K, Taira J, Aoki S. Establishing a parallel compound screening method and identifying novel antimicrobial compounds targeting *Staphylococcus aureus* dihydrofolate reductase. J Appl Pharm Sci, 2022; 12(08):036–047.

SUPPLEMENTARY MATERIAL

Table S1. Accuracy validation results of DUD-E No. 1-102 proteins.

	Protein Name	PDBID	$EF_{2\%}$(GOLD)	$EF_{2\%}$(ADV)	$EF_{2\%}$(PCS)
1	AA2AR	3eml	5	0	2.5
2	ABL1	2hzi	0	7.5	7.5
3	ACE	3bkl	5	0	2.5
4	ACES	1e66	5	5	7.5
5	ADA	2e1w	7.5	2.5	5
6	ADA17	2oi0	2.5	7.5	5
7	ADRB1	2vt4	5	2.5	2.5
8	ADRB2	3ny8	5	0	5
9	AKT1	3cqw	7.5	2.5	5
10	AKT2	3d0e	5	5	5
11	ALDR	2hv5	0	2.5	5
12	AMPC	1l2s	10	2.5	2.5
13	ANDR	2am9	0	10	0
14	AOFB	1s3b	2.5	7.5	5
15	BACE1	3l5d	10	2.5	7.5
16	BRAF	3d4q	5	10	7.5
17	CAH2	1bcd	0	0	0
18	CASP3	2cnk	10	2.5	5
19	CDK2	1h00	5	10	7.5
20	COMT	3bwm	10	2.5	7.5
21	CP2C9	1r9o	7.5	5	5
22	CP3A4	3nxu	2.5	0	0
23	CSF1R	3krj	7.5	2.5	5
24	CXCR4	3odu	0	0	0
25	DEF	1lru	0	2.5	0
26	DHI1	3frj	2.5	5	5
27	DPP4	2i78	5	2.5	2.5
28	DRD3	3pbl	2.5	2.5	5
29	DYR	3nxo	7.5	2.5	7.5
30	EGFR	2rgp	10	2.5	7.5
31	ESR1	1sj0	5	7.5	10
32	ESR2	2fsz	5	5	5
33	FA10	3kl6	7.5	7.5	7.5
34	FA7	1w7x	10	10	10
35	FABP4	2nnq	5	10	10
36	FAK1	3bz3	5	2.5	2.5
37	FGFR1	3c4f	0	0	2.5
38	FKB1A	1j4h	2.5	2.5	0
39	FNTA	3e37	2.5	2.5	0
40	FPPS	1zw5	10	0	0
41	GCR	3bqd	2.5	2.5	5

Continued

	Protein Name	PDBID	$EF_{2\%}$(GOLD)	$EF_{2\%}$(ADV)	$EF_{2\%}$(PCS)
42	GLCM	2v3f	0	0	5
43	GRIA2	3kgc	0	5	5
44	GRIK1	1vso	2.5	0	2.5
45	HDAC2	3max	2.5	5	10
46	HDAC8	3f07	2.5	7.5	2.5
47	HIVINT	3nf7	5	10	10
48	HIVPR	1xl2	7.5	2.5	10
49	HIVRT	3lan	2.5	5	0
50	HMDH	3ccw	7.5	5	10
51	HS90A	1uyg	2.5	0	0
52	HXK4	3f9m	2.5	0	0
53	IGF1R	2oj9	5	7.5	7.5
54	INHA	2h7l	2.5	2.5	2.5
55	ITAL	2ica	0	0	0
56	JAK2	3lpb	2.5	5	5
57	KIF11	3cjo	0	10	2.5
58	KIT	3g0e	2.5	5	7.5
59	KITH	2b8t	7.5	10	10
60	KPCB	2i0e	0	10	5
61	LCK	2of2	0	7.5	5
62	LKHA4	3chp	10	10	10
63	MAPK2	3m2w	5	7.5	10
64	MCR	2aa2	0	2.5	0
65	MET	3lq8	7.5	2.5	7.5
66	MK01	2ojg	10	2.5	10
67	MK10	2zdt	7.5	10	10
68	MK14	2qd9	2.5	2.5	2.5
69	MMP13	830c	2.5	2.5	2.5
70	MP2K1	3eqh	7.5	5	10
71	NOS1	1qw6	10	2.5	7.5
72	NRAM	1b9v	2.5	0	2.5
73	PA2GA	1kvo	7.5	2.5	2.5
74	PARP1	3l3m	2.5	10	10
75	PDE5A	1udt	2.5	2.5	0
76	PGH1	2oyu	2.5	5	2.5
77	PGH2	3ln1	2.5	2.5	7.5
78	PLK1	2owb	0	0	0
79	PNPH	3bgs	5	7.5	5
80	PPARA	2p54	10	2.5	10
81	PPARD	2znp	10	5	7.5
82	PPARG	2gtk	7.5	5	10
83	PRGR	3kba	0	2.5	2.5
84	PTN1	2azr	10	7.5	10

Continued

	Protein Name	PDBID	$EF_{2\%}$(GOLD)	$EF_{2\%}$(ADV)	$EF_{2\%}$(PCS)
85	PUR2	1njs	10	2.5	10
86	PYGM	1c8k	0	5	5
87	PYRD	1d3g	7.5	10	10
88	RENI	3g6z	7.5	2.5	7.5
89	ROCK1	2etr	7.5	0	7.5
90	RXRA	1mv9	10	10	10
91	SAHH	1li4	0	7.5	7.5
92	SRC	3el8	5	5	7.5
93	TGFR1	3hmm	5	7.5	10
94	THB	1q4x	0	7.5	2.5
95	THRB	1ype	7.5	7.5	7.5
96	TRY1	2ayw	7.5	0	7.5
97	TRYB1	2zec	10	2.5	2.5
98	TYSY	1syn	10	10	10
99	UROK	1sqt	10	10	10
100	VGFR2	2p2i	10	7.5	10
101	WEE1	3biz	10	10	10
102	XIAP	3hl5	5	7.5	10